HIPS/ZEOLITE HYBRID COMPOSITES AS ACTIVE PACKAGING MATERIALS: STRUCTURE AND FUNCTIONAL PROPERTIES

European Polymer Journal

Volume 103, June 2018, Pages 88-94

https://doi.org/10.1016/j.eurpolymj.2018.01.013

https://www.sciencedirect.com/science/article/pii/S0014305717317238

Csaba Kenyó[1,2], Károly Renner[1,2,*], János Móczó[1,2], Erika Fekete[1,2] Christoph Kröhnke[3] and Béla Pukánszky[1,2]

[1] Laboratory of Plastics and Rubber Technology, Budapest University of Technology and Economics, H-1521 Budapest, P.O. Box 91, Hungary

[2] Institute of Materials and Environmental Chemistry, Research Centre for Natural Sciences, Hungarian Academy of Sciences, H-1519 Budapest, P.O. Box 286, Hungary

[3] Clariant Produkte (Deutschland) GmbH, D-81477 München, Germany

*Corresponding author: Phone: +36-1-463-2479, Fax: +36-1-463-3474, Email: krenner@mail.bme.hu

ABSTRACT

Desiccant composites were prepared from seven high impact polystyrene copolymers (HIPS) with different butadiene content and dispersed droplet size to study the effect of structure on their functional and application properties. A 4A type zeolite was used as desiccant. The thermodynamic analysis of structure development revealed that the embedding of the zeolite into the polybutadiene droplets is the thermodynamically favored process. Comparison of composite stiffness to theoretically predicted values indicated that considerable embedding occurs during composite preparation. The extent of embedding depends on zeolite content, but also on other factors like butadiene content and the droplet size of the elastomer. Composite stiffness and strength decreases with increasing extent of embedding, while functional properties are dominated by zeolite content. The initial rate of water adsorption increases, while overall rate decreases with increasing desiccant loading. Embedding influences only the initial rate of water adsorption which decreases slightly with increasing extent of encapsulation.

KEYWORDS: Multifunctional composites (A), Particle-reinforcement (A) Physical properties (B), Capacity and rate of water adsorption

1. INTRODUCTION

Plastic packaging materials have been used extensively for the protection and distribution of a wide range of products for a long time. Continuous development resulted in new solutions including functional and smart packaging materials [1-3]. Desiccant packaging controlling the humidity of the ware is extremely important in pharma [4-6] and electronics [7]. Water being present in the atmosphere can be captured either by the adsorption or absorption of water [8]. Absorbents bind moisture as crystal water or they react with it chemically to form a new compound [9-11], while adsorbents are able to bind considerable amount of water on their very large, high energy surface [12-16]. Silica gels [14] and zeolites [17] are applied the most frequently for this latter purpose.

Limited work has been done on factors determining the properties of desiccant composites, or at least very few reports are available in the literature according to our knowledge. Pehlivan et al. [17] studied the water adsorption of PP/zeolite composites and found that adsorption capacities and the rate of water adsorption depended on measurement conditions, which seems to be strange at least. Mathiowitz at al. [14] compared the desiccant effect of a zeolite treated with PEG and compared it to silica gel in PP composites. Their

main conclusion was that zeolite is a more efficient desiccant in such composites than silica gel. One of our previous studies has shown that the adsorption capacity of desiccant composites depends linearly on the amount of the desiccant present, but it is independent of the type of the polymer used [18]. The initial rate of diffusion depends strongly on the specific free volume of the matrix and this factor influences also the overall rate of water adsorption. Both glassy PS and high impact polystyrene (HIPS) have large specific free volume and they are successfully used as matrices for desiccant composites. The results of another study indicated that dispersed structure and elastomer content might influence both functional and application properties [19], but the effect of these factors on composite properties has never been investigated before.

HIPS prepared by suspension polymerization has a complicated, salami like structure consisting of a polystyrene matrix with dispersed polybutadiene droplets, which, on the other hand, contain small PS inclusions [20]. Adding a filler, like zeolite, to this material may increase the complexity of structure further. Multicomponent, hybrid materials have been prepared earlier, and in fact they are used extensively in industrial practice today [21-30]. The stiffness of polypropylene (PP), for example, is increased by adding a filler (talc, $CaCO_3$, short glass fibers), while its impact

resistance is improved by the incorporation of an elastomer to produce bumper materials [31,32]. Two boundary structures may develop in such materials; the components can be dispersed in the PP matrix separately from each other or the filler can be encapsulated by the elastomer to form embedded structure. The actual structure developing depends on the balance of adhesion and shear forces prevailing during the processing of the material [23]. Properties are determined by structure, composites with embedded morphology have smaller stiffness than those with the separate distribution of the components. Structure development, and the relationship between structure and properties has not been studied much in PS or HIPS composites up to now; very few reports are available in the literature. Siengchin and Karger-Kocsis [29] observed embedded structure in PS/SBR/boehmite composites, while Chang et al. [30] controlled structure by the use of functionalized polymer. They prepared HIPS/elastomer/$Mg(OH)_2$ composites using SEBS or SEBS-g-MA to achieve separately distributed or embedded structure, respectively. However, no study has been done and results reported on HIPS/zeolite desiccant composites yet. As a consequence, the goal of our work was to investigate structure development in such composites, determine the extent of embedding, if it occurs, and find correlations between the structure and functional properties of the composites, if they exist. Seven different HIPS polymers with dissimilar butadiene

content and dispersed particle size were used as matrices and a standard 4A type zeolite as desiccant in the study.

2. EXPERIMENTAL

2.1. Materials

The seven high impact copolymers used were characterized with a variety of methods before using them as matrix in the experiments. The polymers with the trade name "Styron" were obtained from Dow, USA, while those named "Empera" from Ineos Nova, Switzerland. The grades used, the abbreviations applied and the most important characteristics are listed in **Table 1**. Instead of the trade name we use ten times the butadiene content in the abbreviation of the HIPS copolymers. Butadiene content was determined by the measurement of the iodine value according to the ASTM D 5902-2005 standard; unsaturations were reacted with iodine chloride in chloroform and the residual chloride was titrated with sodium thiosulfate. The molecular weight of the polymers was determined by gel permeation chromatography in THF using a Waters e2695 Separation Module. The measurements were done at 35 °C with 0.5 ml/min flow rate using Styragel columns. Calibration was done with polystyrene standards. Density was measured using a pycnometer at room temperature. The water vapor transmission rate (WVTR) of the polymers was determined on 100 μm thick films using a Mocon Permatran W1A equipment. Results were calculated for 20 μm

thickness according to industrial practice. The structure of the copolymers was studied by transmission electron microscopy (TEM). 100 nm thick slices were cut at -100 °C with a Leica EM UC6 Ultramicrotome and then stained with osmium tetroxide for 4 hours. Micrographs were recorded with a FEI Morgagni 268D electron microscope. Structure, size and size distribution of polybutadiene droplets were determined from the micrographs by image analysis using the Image Pro Plus 6 software (Media Cybernetics, USA). The average particle size of dispersed butadiene particles is also collected in **Table 1**.

The zeolite 4A used as desiccant was obtained from the Luoyang Jianlong Chem. Ind. Co., China. Its water adsorption characteristics were determined in an atmosphere of 100 % relative humidity by the measurement of the weight of the samples as a function of time. Pore size and volume were characterized by water adsorption using a Hydrosorb (Quantachrome, USA) apparatus at 20 °C. The sample was evacuated at 300 °C for 24 hours down to 10^{-5} Hgmm before measurement. The particle size and size distribution of the zeolite were determined using a Malvern Mastersizer 2000 equipped with a Sirocco powder analyzer. The density of the zeolite was measured by helium pycnometry. The average particle size of the desiccant is 4.0 μm, its density 1.7 g/cm^3 and its theoretical pore diameter 3.8 Å.

2.2. Sample preparation

Before composite preparation the zeolite was dried at 300 °C for 16 h in vacuum. The components were homogenized in a Brabender W 50 EH internal mixer with roller blades attached to a Haake Rheocord EU 10 V driving unit at 190 °C for 10 min. 1 mm thick plates and 100 μm thick films were compression molded from the homogenized material at 190 °C using a Fontijne SRA 100 equipment immediately after removing the melt from the chamber of the internal mixer.

2.3. Measurements

The water adsorption of the composites was determined by the measurement of weight in an atmosphere of 100 % RH on 20 x 20 x 1 mm specimens as a function of time. Their zeolite content was checked by thermal gravimetry (TGA, Perkin Elmer TGA 6). 15 mg samples were heated to 650 °C with 80 °C/min rate in oxygen and kept there for 5 min to burn off the polymer. The surface tension of the polymers was determined by static contact angle measurements. Normal alkanes were used for the determination of the dispersion component of surface tension, while six different solvents (water, glycerol, ethylene glycol, dimethyl sulfoxide, formamide, and 1-bromo-naphthalene) were applied for the estimation of the polar component. An attempt was made to determine the surface tension of the zeolite by inverse gas chromatography (IGC,

Perkin Elmer Autosystem XL gas chromatograph). The filler was agglomerated with water and the 800-1200 μm fraction was used for the packing of the column. The dispersion component of surface tension was determined by the injection of n-alkanes at various temperatures between 200 and 280 °C. Unfortunately, none of the polar solvent eluted from the column thus the polar component of surface tension of the zeolite could not be determined with this method. On the other hand, we could calculate this characteristic from spreading pressure derived from the adsorption isotherm of water on the zeolite. Mechanical properties were characterized by tensile testing using an Instron 5566 machine at 115 mm gauge length and 5 mm/min cross-head speed on specimens with 1 x 10 mm dimensions. Notched Charpy impact resistance was determined according to the ISO 179 standard at 23 with 2 mm notch depth. The distribution of the zeolites in the composites was studied by scanning electron microscopy using a Jeol JSM 6380 LA apparatus. Micrographs were recorded on sputter coated fracture surfaces created during tensile testing.

3. RESULTS AND DISCUSSION

The results are presented in three sections. First the thermodynamics of structure formation is considered and then the structure actually developed is discussed in the next section. Correlations between structure and properties are

presented subsequently with a brief reference to consequences for practice in the last section.

3.1. Thermodynamics

As mentioned in the introductory part the structure of multicomponent materials containing an elastomer and a filler is rather complex and two boundary structures, separate dispersion and encapsulation, may form in them during processing. Embedding is the more complicated of the two, since certain conditions must be fulfilled in order to form such a highly ordered structure. Zeolite particles and elastomer droplets must meet and collide, energy balance must be favorable and the formed structure must be stable and withstand the effect of shear. De-encapsulation was shown to occur in a considerable number of composites [33].

Physicochemical processes occur spontaneously only in cases when the energy balance is advantageous, the change in free energy is negative. Composite preparation and blending results in new surfaces which require surplus energy, thus the change of free energy is positive. The increase in free energy depends on the size of the contact surface and interfacial tension; both are different in the case of separate dispersion and during embedding. At constant volume surface energy can be related to surface tension in the following way

$$U^S = A^S - T\left(\frac{\partial A^S}{\partial T}\right)_v = \gamma - T\frac{\mathrm{d}\lambda}{\mathrm{d}T} \qquad (1)$$

where U^S and A^S are the surface energy and surface free energy of a unit surface, respectively, and γ is surface tension. **Equation 1** is valid for gases and liquids for which complete reversibility can be assumed [34]. Nevertheless, we can use the equation for qualitative, comparative purposes and neglect the lack of complete reversibility in solids. The change in surface energy during structure formation is proportional to interfacial tension which can be calculated from the geometric mean correlation of Wu [35]

$$\gamma_{AB} = \gamma_A + \gamma_B - 2\left(\gamma_A^d \gamma_B^d\right)^{1/2} - 2\left(\gamma_A^p \gamma_B^p\right)^{1/2} \qquad (2)$$

where γ_{AB} is interfacial tension, γ_A and γ_B are the surface tensions of the two materials in contact, and d and p stand for the dispersion and polar components of surface tension.

The surface tension of the components are listed in **Table 2**. We can see that the surface energy of zeolite is much larger than that of the polymers with a significant polar component. The knowledge of surface tension allows the calculation of interfacial tension according to **Eq. 2** for both possible cases. In the case of separate dispersion PS/PB and PS/zeolite surfaces must be considered, while PS/PB and PB/zeolite surfaces form when embedding occurs. The calculations were carried out for the composition of 20 vol% zeolite and 10 vol% polybutadiene content. We assumed that in a unit volume of the composite the interface between the matrix and the filler equals to the surface area of the zeolite (average particle

size is 4.0 µm, outer surface area 2.3 m^2/g) and that the average diameter of the elastomer is 1 µm (**see Table 1**). Furthermore, we assumed that the zeolite is covered only on its outer surface by the elastomer, it does not penetrate into its pores. Finally, we neglected the PS inclusions inside the elastomer droplets during these model calculations. According to these calculations the surplus energy needed for the creation of new surfaces is 353.0 kJ/m^3 in the case of separate dispersion and 323.1 kJ/m^3 for embedding. The difference is 29.9 kJ/m^3 in favor of embedding, i.e. the embedded structure is energetically favored like in several other cases [23,36,37]. Accordingly, we must expect the encapsulation of zeolite within the elastomer thus resulting in a complex morphology, since exclusive structures have never been observed before even when functionalized polymers were used to promote one structure or the other [24-26,28,38-40]. The occurrence of embedding and its effect on properties are discussed in the following sections.

3.2. Structure

The main question of structure formation is the occurrence and extent of embedding, as discussed above. Attempts can be made to check encapsulation with the help of electron microscopy [22,26,27], but sample preparation and especially interpretation are not straightforward. A much

better indication of embedding is the decrease of stiffness. Filler particles embedded into the elastomer extend the volume of the latter, i.e. they act like elastomer droplets and decrease stiffness. The phenomenon is demonstrated in **Fig. 1** in which the Young's modulus of two series of composites is plotted as a function of zeolite content. Two lines are also added to the figure; the upper one corresponds to the separate dispersion of the components, while the lower one to complete embedding. The stiffness of the two series prepared with the HIPS120 and HIPS104 matrices, respectively, is located between the two boundary lines indicating certain, but not complete embedding. The extent of embedding can be deduced from deviation from the boundary cases; **Fig. 1** shows that it is larger for the HIPS120 than for the other material plotted. Obviously, larger butadiene content and larger size of the dispersed elastomer droplets favor embedding (**see Table 1**).

The extent of embedding can be calculated with the help of appropriate models. In the case of separate dispersion the composition dependence of Young's modulus, $E(\varphi)$, can be expressed by the extension of the Kerner-Nielsen equation [41]

$$E_c(\varphi) = E_m \frac{1 + A_f B_f \varphi_b}{1 - \Psi_f B_f \varphi_b} \frac{1 - \Psi_e B_e \varphi_e}{1 + A_e B_e \varphi_e} \qquad (3)$$

where E_m is the modulus of the matrix polymer, φ_f and φ_e are the volume fraction of the zeolite and the elastomer, respectively. A_f and A_e take the form

$$A_f = \frac{7 - 5\nu_m}{8 - 10\nu_m} \quad \text{and} \quad A_e = \frac{8 - 10\nu_m}{7 - 5\nu_m} \tag{4}$$

where ν_m is the Poisson's ratio of the neat matrix. Parameter B_f and B_e can be calculated as

$$B_f = \frac{E_f / E_m - 1}{E_f / E_m + A_f} \quad \text{and} \quad B_e = \frac{E_m / E_e - 1}{E_m / E_e + A_e} \tag{5}$$

Ψ is a correction factor taking into account the maximum packing fraction (φ_{max}) of the inclusion and it takes the same form for the filler and the elastomer

$$\Psi_f = 1 + \left(\frac{1 - \varphi_f^{\max}}{\varphi_f^{\max 2}} \right) \varphi_f \tag{6}$$

Naturally always the appropriate volume fraction and φ^{max} value must be introduced into **Eq. 6**. Deviation of measured stiffness from the one calculated for separate dispersion (see corresponding line in **Fig. 1**) allows the calculation of the volume fraction of embedded particles. The parameters used in the calculations are collected in **Table 3**. The Poisson's ratio of neat PS was taken as 0.34 and its modulus as 3.2 GPa. During the calculation and analysis we ignored the amount of PS particles embedded already within the elastomer droplets, since the actual value of matrix stiffness takes it into account.

The extent of embedding was calculated for all the composites prepared and it is plotted against butadiene

content at three different zeolite content in **Fig. 2**. The extent of embedding decreases with increasing zeolite content non-linearly as shown by the figure. The compositions plotted were selected accordingly. The continuous lines are drawn only to guide the eye in this and in all other figures, they are not fitted correlations. The tendency shown is easy to understand since the amount of elastomer is limited, it has a certain capacity to embed zeolite particles. At small zeolite and comparatively large polybutadiene content the probability of encapsulation is large. The figure clearly shows also that embedding increases with increasing elastomer content that also seems to be evident. The effect of elastomer content diminishes with increasing zeolite content probably due to the saturation of the droplets by zeolite particles. However, some other factor or factors also influences the extent of embedding shown by the position of the HIPS67 matrix, in which embedding is relatively small. This other factor might be the particle size of the elastomer droplets. The extent of embedding is plotted against this variable in **Fig. 3**. A tendency exists indeed, but some deviating points can be observed again. HIPS65 has the smallest particle size and relatively small butadiene content, but the extent of embedding is relatively large in it, while HIPS67 has practically the same elastomer content and larger size, still embedding is very small. Further study and analysis is needed

to reveal the reason for the deviations from the general tendency and to find the parameters determining the extent of embedding.

3.3. Properties

We established in the previous sections that embedding is thermodynamically favored and really occurs in the HIPS/zeolite composites prepared in the study. The questions remains about the effect of structure on the application and functional properties of the composites. Young's modulus is plotted against the extent of embedding in **Fig. 4**. A clear effect is seen, stiffness decreases considerably with increasing extent of embedding. However, the correlation must be treated with caution, since the extent of embedding depends also on zeolite content (see **Figs. 2 and 3**), thus **Fig. 4** is biased by this dependence. Nevertheless, the effect of embedding exists and can be seen clearly if we compare the various polymers at the same zeolite content; modulus decreases with increasing extent of embedding indeed and the effect is stronger at larger filler content. A similar, but less strong and clear correlation is obtained if we investigate the dependence of tensile strength on the extent of embedding (**Fig. 5**). Deviations from the general tendency are larger than for stiffness, but tensile strength clearly

decreases with increasing extent of embedding. We must also mention here that deformability increases slightly at the same time (not shown), which might be advantageous for several applications since it increases the fracture resistance of the material.

The effect of embedding on application properties is more advantageous than not, but encapsulation may influence functional properties, i.e. the capacity and rate of water adsorption as well. We have shown earlier that the main factor determining the water adsorption capacity of polymer/zeolite composites is their desiccant content; capacity increases linearly with the amount of zeolite used [31, 42]. The capacity of water adsorption is plotted against the extent of embedding in **Fig. 6**. The correlation is strongly biased again by changing zeolite content. A closer scrutiny of values measured at the same zeolite loading reveals that embedding practically does not influence the water adsorption capacity of the desiccant composites studied.

The rate of water adsorption was determined by the measurement of weight as a function of time in an atmosphere of 100 % relative humidity. The results were fitted with models assuming Fickian diffusion. The overall rate of water adsorption was characterized by parameter *a* deduced from the following correlation

$$M_t = M_\infty \left(1 - \frac{8}{\pi^2}\left(\exp(-a\,t) + \frac{1}{9}\exp(-9\,a\,t) + \frac{1}{25}\exp(-25\,a\,t)\right)\right) \qquad (7)$$

where M_t is time dependent weight increase, M_∞ the final water uptake reached after infinite time (adsorption capacity), a (1/s) a constant characterizing the overall rate of water adsorption and t the time of adsorption . The initial rate of adsorption can be derived from a different form of Fick's law

$$\frac{M_t}{M_\infty} = 4\left(\frac{D\,t}{L^2}\right)^{1/2}\left(\pi^{-1/2} + 2\sum_{m=0}^{\infty}(-1)^m ierfc\frac{m\,L}{2\,(D\,t)^{1/2}}\right) \qquad (8)$$

where D is diffusion coefficient and L the thickness of the sample. If we plot water uptake as a function of the square root of time, we should obtain a straight line the slope of which, b ($s^{-1/2}$), is proportional to the initial rate of water adsorption.

The overall rate of adsorption is plotted again the extent of embedding in **Fig. 7** and it decreases with increasing zeolite content in accordance with earlier observations [31]. This composition dependence was explained by the increase of diffusion path with increasing desiccant content. However, if we disregard the effect of zeolite content we do not see any clear tendency as a function of embedding. On the other hand, some factor or factors influence the overall rate of water adsorption significantly, since relatively large scatter is observed within each group of values at the same zeolite content. These factors might be butadiene content, particle size or even the extent of embedded PS. The initial rate of water adsorption, on the other hand, changes differently, it

increases with increasing zeolite content (**Fig. 8**). The effect of embedding is somewhat smaller, but exists, diffusion rate decreases with increasing extent of encapsulation. This can be seen especially well if we follow the tendency at 30 vol% desiccant content (▽). The explanation for the decreased initial rate of water adsorption is not evident at all. Butadiene is an elastomer with low glass transition temperature and large mobility of the molecules at room temperature. The rate of diffusion is large in such materials, since the rate determining process is diffusion through the matrix PS. We might assume that the elastomer molecules penetrate the pores of the zeolite, but this is not very probable and we do not have any evidence for it. A further, more detailed study is needed to reveal the reason for the decrease in the initial rate of water adsorption with increasing extent of embedding.

4. CONCLUSIONS

Desiccant composites were prepared from seven high impact polystyrenes with different butadiene contents and dispersed droplet sizes and a 4A type zeolite in a wide range of desiccant contents. Thermodynamic analysis of structure development revealed that the embedding of the zeolite into the polybutadiene droplets is the thermodynamically favored process. Comparison of composite stiffness to theoretically

predicted values indicated that considerable embedding occurs during composite preparation. The extent of embedding depends on zeolite content, but also on other factors like butadiene content and the droplet size of the elastomer. Further unidentified factors also influence the extent of embedding. Composite stiffness and strength decreases with increasing extent of embedding. Functional properties are dominated by zeolite content. The water adsorption capacity of HIPS/zeolite desiccant composites depends almost exclusively on zeolite content. The initial rate of water adsorption increases, while the overall rate decreases with increasing desiccant loading. Embedding influences only the initial rate of water adsorption which decreases slightly with increasing extent of encapsulation. The influence of embedding is slightly favorable for application properties, while embedding practically does not affect functional properties thus HIPS is a very advantageous matrix for the production of desiccant composites.

5. ACKNOWLEDGEMENTS

The authors are indebted to Levente Kovács and Dániel Bedő for the execution of the WVTR measurements, to Ádám Gyürki for sample preparation, to Krisztina László-Nagy and Ajna Tóth for the adsorption measurements. The research on heterogeneous polymer systems was financed by National Scientific Research

Fund of Hungary (OTKA Grant No. K 120039, K 108934 and PD 112489) and partly by the former Süd-Chemie AG, today Clariant, Business Unit Masterbatches on functional packaging materials; we appreciate the support very much. One of the authors (KR) is grateful also to the János Bolyai Research Scholarship of the Hungarian Academy of Sciences.

6. REFERENCES

1. Rooney ML. Active food packaging; Blackie Academic & Professional: London, 1995.
2. Brody AL, Strupinsky ER, Kline LR. Active Packaging for Food Applications; CRC Press: London, New York, 2001.
3. Day BPF. Active packaging - a fresh approach. J Brand Technol 2001;1,32-41.
4. Allinson JG, Dansereau RJ, Sakr A. The effects of packaging on the stability of a moisture sensitive compound. Int J Pharm 2001;221,49-56.
5. Waterman KC, MacDonald BC. Package selection for moisture protection for solid, oral drug products. J Pharm Sci 2010;99,4437-4452.
6. Naveršnik K, Bohanec S. Predicting drug hydrolysis based on moisture uptake in various packaging designs. Eur J Pharm Sci 2008;35,447-456.
7. Wong EH, Rajoo R. Moisture absorption and diffusion characterisation of packaging materials--advanced treatment. Microelectron Reliab 2003;43,2087-2096.
8. Ruthven DM. Principles of Adsorption and Adsorption Processes; John Wiley & Sons: New York, 1984.
9. Imre B, Keledi G, Renner K, Móczó J, Murariu M, Dubois P, Pukánszky B. Adhesion and micromechanical

deformation processes in PLA/CaSO4 composites. Carbohydr Polym 2012; 89,759-767.

10. Nji J, Li G. A CaO enhanced rubberized syntactic foam. Composites A 2008;39,1404-1411.
11. Ovoshchnikov DS, Glaznev IS, Aristov YI. Water sorption by the calcium chloride/silica gel composite: The accelerating effect of the salt solution present in the pores. Kinet Catal 2011;52,620-628.
12. Kim H, Biswas J, Choe S. Effects of stearic acid coating on zeolite in LDPE, LLDPE, and HDPE composites. Polymer 2006;47,3981-3992.
13. Liu Q, De Kee D, Gupta RK. Models of moisture diffusion through vinyl ester/clay nanocomposites. AIChE J., 2008;54,364-371.
14. Mathiowitz E, Jacob JS, Jong YS, Hekal TM, Spano W, Guemonprez R, Klibanov AM, Langer R. Novel desiccants based on designed polymeric blends. J Appl Polym Sci 2001;80,317-327.
15. Ragosta G, Abbate M, Musto P, Scarinzi G, Mascia L. Epoxy-silica particulate nanocomposites: Chemical interactions, reinforcement and fracture toughness. Polymer 2005;46,10506-10516.
16. Spahis N, Dellali M, Mahmoudi H. Synthesis and Characterization of Polymeric/Activated Carbon Membranes. Procedia Eng 2012;33,47-51.
17. Pehlivan H, Özmıhçı F, Tıhmınlıoğlu F, Balköse D, Ülkü S. Water and water vapor sorption studies in polypropylene–zeolite composites. J. Appl. Polym. Sci., 2003;90,3069-3075.
18. Kenyó C, Kajtár DA, Renner K, Kröhnke C, Pukánszky B. Functional packaging materials: factors affecting the capacity and rate of water adsorption in desiccant composites. J Polym Res 2013;20,294-302.

19. Kenyó C, Renner K, Móczó J, Fekete E, Kröhnke C, Pukánszky B. Effect of desiccant characteristics on the properties of PS/zeolite functional packaging materials. Polym Compos 2014;35(11),2112-2120.
20. Bucknall CB. Toughened Plastics, Applied Science Publishers, Ltd., London 1977.
21. Kolárik J, Lednicky F, Pukánszky B. Ternary composites polypropylene/ elastomer/filler: structure and elastic properties. in Proceeding of the 6th ICCM/2nd ECCM, London, Elsevier 1987.
22. Kolárik J, Lednicky F, Jancár J, Pukánszky B. Phase-structure of ternary composites consisting of polypropylene elastomer filler - effect of functionalized components. Polym Commun 1990;31(5),201-204.
23. Pukánszky B, Tüdős F, Kolárik J, Lednicky F. Ternary composites of polypropylene, elastomer, and filler - analysis of phase-structure formation. Polym Compos 1990;11(2),98-104.
24. Hornsby PR, Premphet K. Influence of phase microstructure on the mechanical properties of ternary phase polypropylene composites. J Appl Polym Sci 1998;70(3), 587-597.
25. Premphet K, Horanont P. Influence of stearic acid treatment of filler particles on the structure and properties of ternary-phase polypropylene composites. J Appl Polym Sci 1999;74(14),3445-3454.
26. Premphet K, Horanont P. Phase structure of ternary polypropylene/elastomer/filler composites: effect of elastomer polarity. Polymer 2000;41(26),9283-9290.
27. Premphet K, Horanont P. Phase structure and property relationships in ternary polypropylene/elastomer/filler composites: Effect of elastomer polarity. J Appl Polym Sci 2000;76(13),1929-1939.

28. Hikasa S, Nagata K, Nakamura Y. Influences of morphology on mechanical properties of polypropylene/ elastomer/CaCO3 ternary composites. Compos Interfaces 2011;18(1),1-22.
29. Siengchin S, Karger-Kocsis J. Binary and ternary composites of polystyrene, styrene–butadiene rubber and boehmite produced by water-mediated melt compounding: Morphology and mechanical properties. Compos Part B 2013;45(1),1458-1463.
30. Chang S, Xie T, Yang G. Morphology and mechanical properties of highimpact polystyrene/elastomer/magnesium hydroxide composites. J Appl Polym Sci 2006;102(6),5184-5190.
31. Nishio T, Nomura T, Kawamura N, Sato H, Uchikawa A, Tsutsumi I, Goto Y. Ethylene-propylene copolymer, ethylene copolymer, propylene polymer and talc. US 5374677 1994.
32. Kobayashi Y, Kusuyama H, Machida S, Tanaka A. Polyolefin resin composition. EP 0831125 2004.
33. Sudár A, Burgstaller C, Renner K, Móczó, J, Pukánszky B. Wood fiber reinforced multicomponent, multiphase PP composites: Structure, properties, failure mechanism. Compos Sci Technol 2014;103,106-112.
34. Adamson AW, Gast AP. Physical Chemistry of Surfaces. 6th ed., John Wiley & Sons, New York 1997.
35. Wu S. Interfacial and surface tensions of polymers. J Macromol Sci Part C 1974;10(1), 1-73.
36. Kolárik J, Lednický F. Structure of polypropylene/EPDM elastomer/calcium carbonate composites. in Polymer Composites, Sedlácek, B., Walter de Gruyter, Berlin 1986.
37. Pukánszky B, Kolárik J, Lednicky F. Mechanical properties of threecomponent polypropylene composites.

in Polymer Composites, Sedlácek, B., Walter de Gruyter, Berlin 1986.

38. Qiu W, Zhang F, Endo T, Hirotsu T. Preparation and characteristics of composites of high-crystalline cellulose with polypropylene: effects of maleated polypropylene and cellulose content. J Appl Polym Sci 2003;87(2),337-345.
39. Ariffin A, Mansor AS, Jikan SS, Ishak ZAM. Mechanical, morphological, and thermal properties of polypropylene/kaolin composite. Part I. The effects of surface-treated kaolin and processing enhancement. J Appl Polym Sci 2008;108(6),3901-3916.
40. Wang YJ, Chen S, Shi YQ, Dong YX, Fu LD, Xu XB, Wang X. Mechanical properties and tensile deformation behavior of polyamide 6/maleated and unmaleated ethylene propylene diene terpolymer/nano-CaCO3 Ternary Composites. J Macromol Sci Part B 2013;52(6),797-811.
41. Nielsen LE. Mechanical Properties of Polymers and Composites. Marcel Dekker, New York 1974.
42. Kenyó Cs, Hári J, Renner K, Kröhnke C, Pukánszky B. Effect of Matrix Characteristics on the Properties of High-Impact Polystyrene/Zeolite Functional Packaging Materials. Ind Eng Chem Res 2014;53,19208–19215.

Table 1 The most important characteristics of the polymers used in the experiments

Polymer	Abbrev.	PB content (vol%)	Particle size (μm)	MFI[a] (g/10 min)	M_n (g/mol)	M_w/M_n	Impact strength (kJ/m^2)	WVTR (g 20 μm/m^2/24 h)
Styron 485	HIPS67	6.7	1.2 ± 0.7	12.0	77525	2.68	7.0	139 ± 2
Styron 1175	HIPS86	8.6	2.6 ± 2.3	2.8	95840	2.54	11.0	151 ± 7
Styron 1200	HIPS98	9.8	1.0 ± 0.5	5.0	79 420	2.04	12.0	154 ± 13
Empera 416	HIPS47	4.7	1.7 ± 0.8	21.0	85 640	2.17	5.0	107 ± 4
Empera 524	HIPS65	6.5	0.6 ± 0.2	10.5	81 890	2.79	8.0	145 ± 5
Empera 613	HIPS120	12.0	2.4 ± 1.2	6.0	78 760	2.29	9.5	167 ± 19
Empera 622	HIPS104	10.4	1.5 ± 0.7	4.8	84 490	2.14	10.0	166 ± 2

a) 200 °C, 5 kg

Table 2 Surface tension of the components used in the model calculations of structure development

Material	Surface tension (mJ/m^2)		
	γ^d	γ^p	γ
Polystyrene	40.5	1.1	41.6
Polybutadiene	32.9	5.0	37.9
Zeolite	181.9	440.9	622.8

Table 3 Parameters used in the calculation of the extent of embedding (see **Eqs. 3-6**)

Parameter	Zeolite	Polybutadiene
Modulus, *E* (GPa)	25.0	0.002
Parameter *A*	1.152	0.868
Parameter *B*	0.760	0.999
Maximum packing fraction, φ^{max}	0.70	0.64

7. CAPTIONS

Fig. 1 Young's modulus of HIPS desiccant composites plotted as a function of zeolite content. Indication of embedding. Symbols: (○) HIPS120, (□) HIPS104; the upper and lower continuous lines represent the boundary structures of separate dispersion and complete embedding, respectively.

Fig. 2 Effect of zeolite and polybutadiene content on the extent of embedding in HIPS/zeolite desiccant composites. Symbols: (○) 10, (□) 20, (△) 50 vol% zeolite.

Fig. 3 Dependence of the extent of embedding on the size of the dispersed polybutadiene particles. Symbols: (○) 10, (□) 20, (△) 50 vol% zeolite.

Fig. 4 Influence of the extent of embedding on the stiffness of HIPS/zeolite desiccant composites. Symbols: (○) 10, (□) 20, (▽) 30, (◇) 40, (△) 50 vol% zeolite.

Fig. 5 Correlation between the tensile strength of HIPS/zeolite desiccant composites and the extent of embedding. Symbols: (○) 10, (□) 20, (▽) 30, (◇) 40, (△) 50 vol% zeolite.

Fig. 6 Effect of the extent of embedding on the water adsorption capacity of HIPS/zeolite composites. Symbols: (○) 10, (□) 20, (▽) 30, (◇) 40, (△) 50

vol% zeolite.

Fig. 7 Loose correlation between the overall rate of water adsorption and the extent of embedding in HIPS/zeolite desiccant composites. Symbols: (○) 10, (□) 20, (▽) 30, (◇) 40, (△) 50 vol% zeolite.

Fig. 8 Influence of the extent of embedding and zeolite content on the initial rate of water adsorption in HIPS/zeolite desiccant composites. Symbols: (○) 10, (□) 20, (▽) 30, (◇) 40, (△) 50 vol% zeolite.

Kenyó, Fig. 1

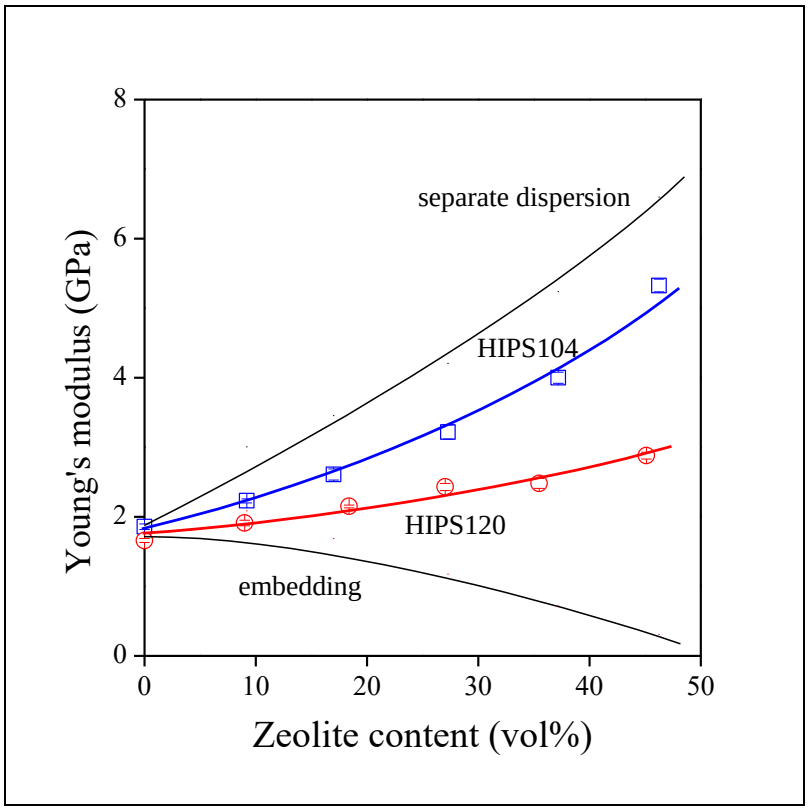
Young's modulus (GPa)
Zeolite content (vol%)
separate dispersion
HIPS104
HIPS120
embedding
0
2
4
6
8
0
10
20
30
40
50

Kenyó, Fig. 2

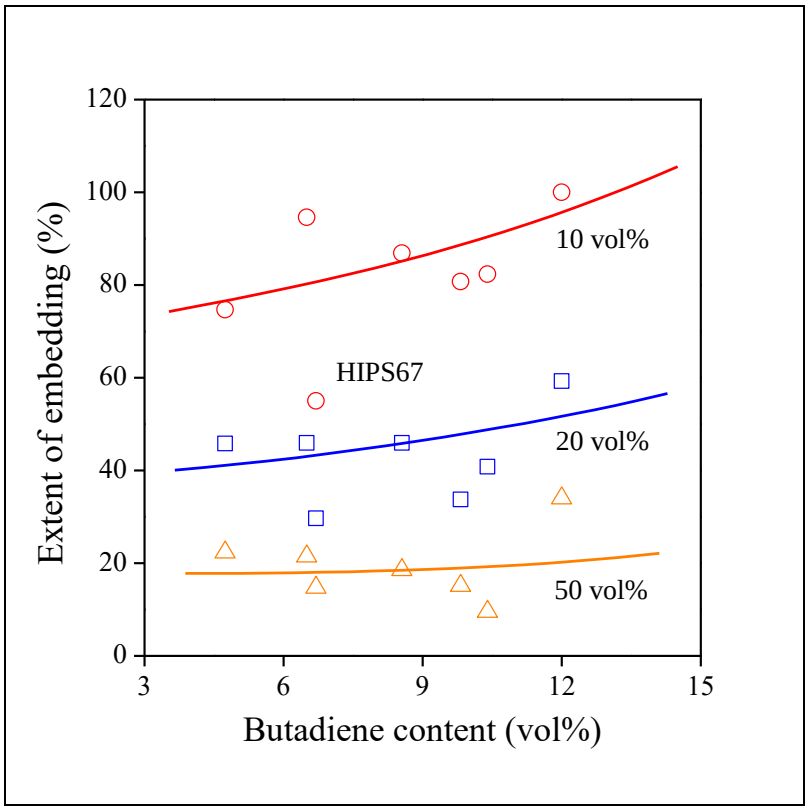
Extent of embedding (%)
120
100
80
60
40
20
0
3
6
9
12
15
Butadiene content (vol%)
10 vol%
HIPS67
20 vol%
50 vol%

Kenyó, Fig. 3

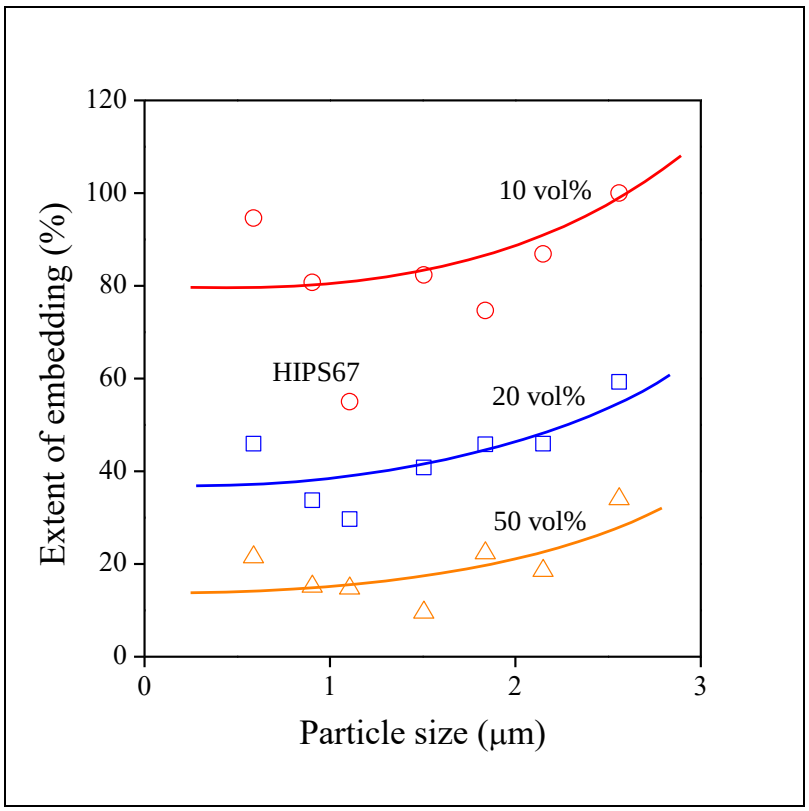
Extent of embedding (%)
120
100
80
60
40
20
0
0
1
2
3
Particle size (μm)
10 vol%
HIPS67
20 vol%
50 vol%

Kenyó, Fig. 4

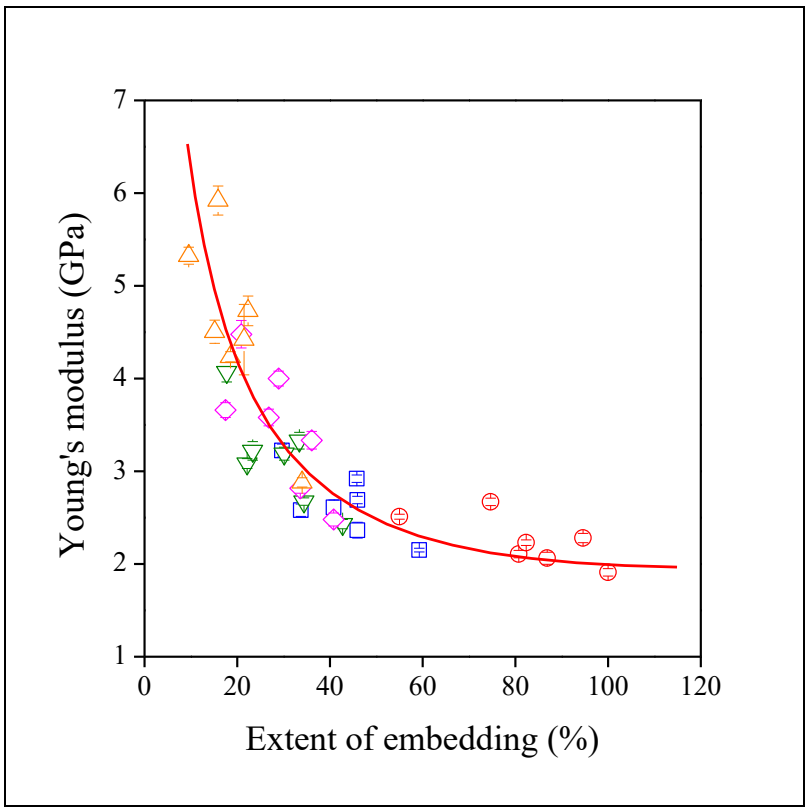
Young's modulus (GPa)
Extent of embedding (%)
1
2
3
4
5
6
7
0
20
40
60
80
100
120

Kenyó, Fig. 5

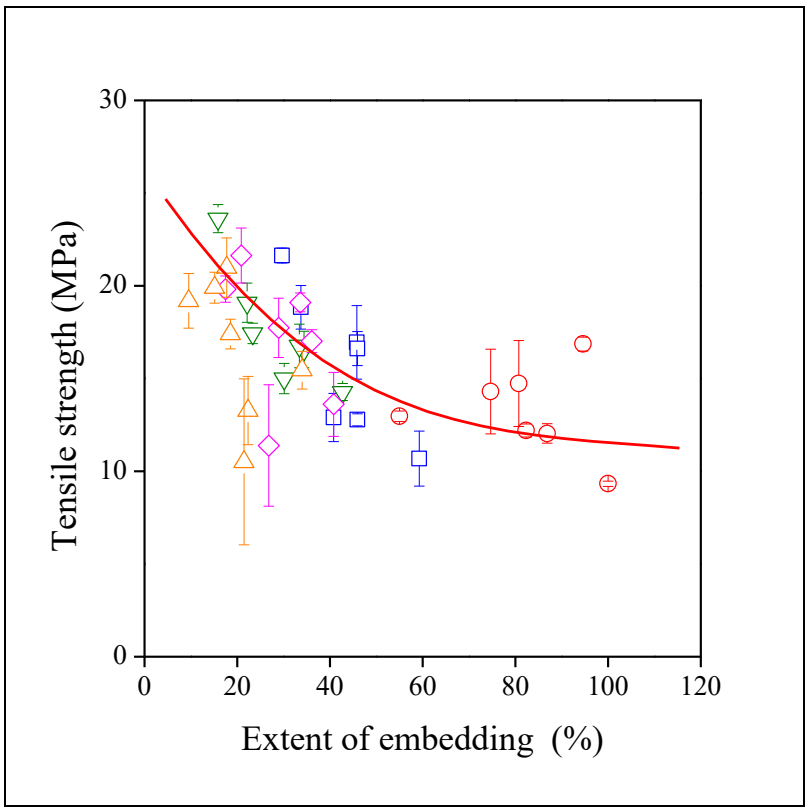
Tensile strength (MPa)
30
20
10
0
0
20
40
60
80
100
120
Extent of embedding (%)

Kenyó, Fig. 6

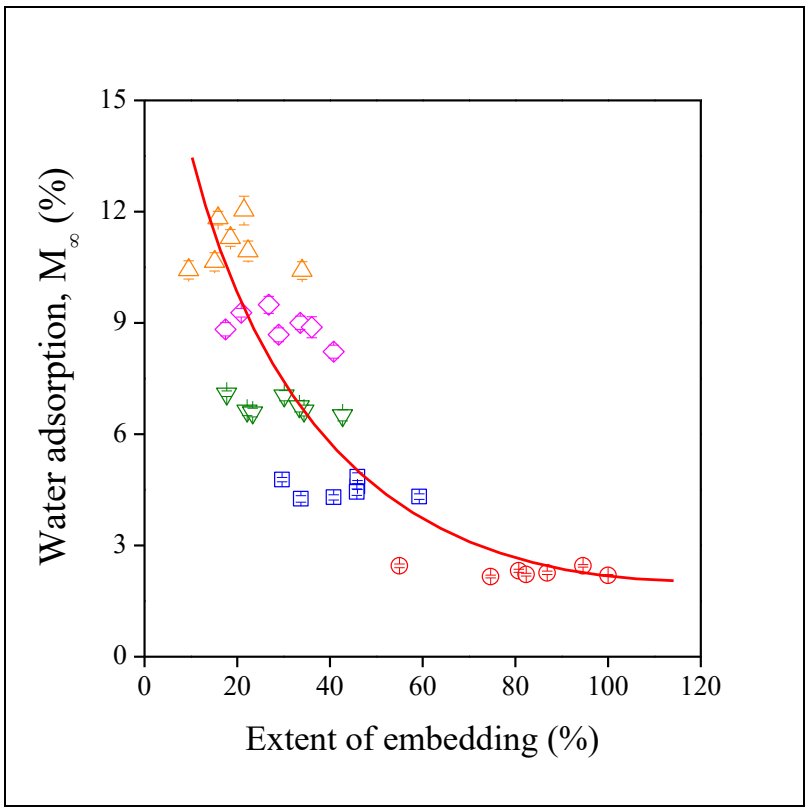
Water adsorption, M_∞ (%)
Extent of embedding (%)
0
3
6
9
12
15
0
20
40
60
80
100
120

Kenyó, Fig. 7

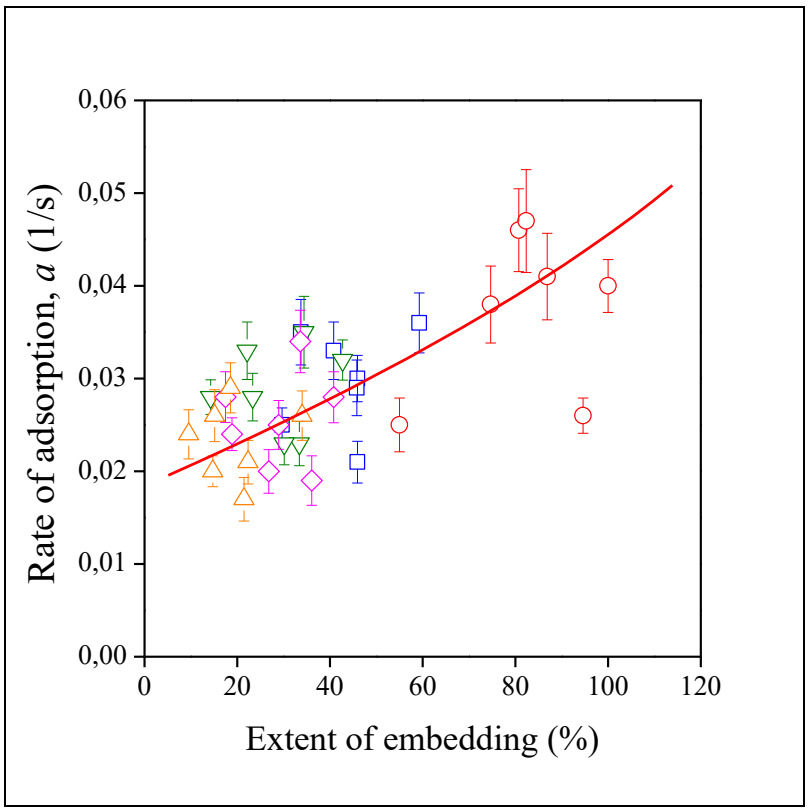
Rate of adsorption, a (1/s)
0,06
0,05
0,04
0,03
0,02
0,01
0,00
0
20
40
60
80
100
120
Extent of embedding (%)

Kenyó, Fig. 8

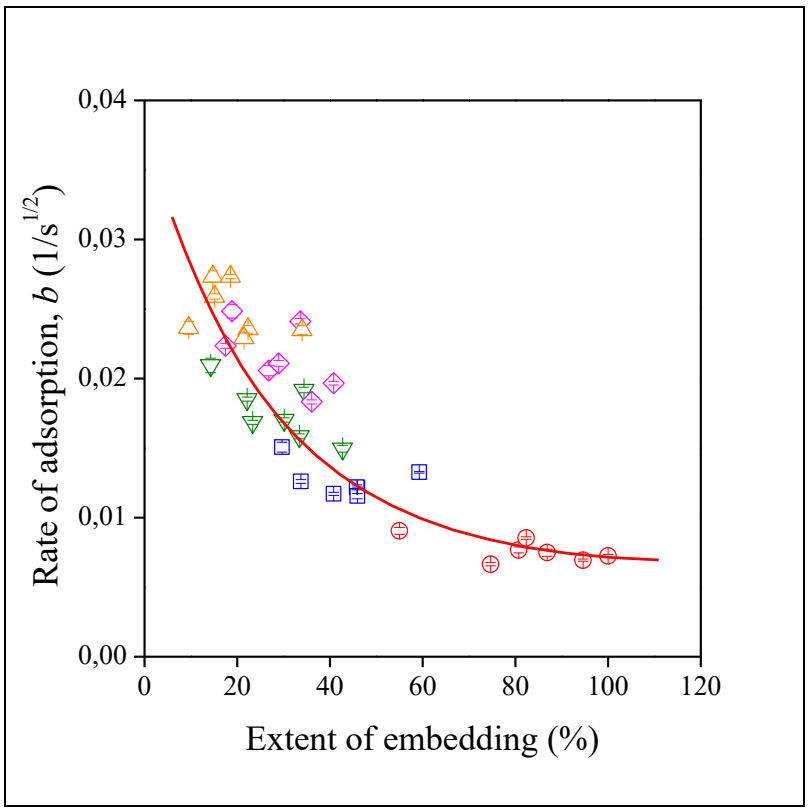
0,04
0,03
0,02
0,01
0,00
Rate of adsorption, b (1/s^1/2)
0
20
40
60
80
100
120
Extent of embedding (%)